

Investigation of 3D printed lightweight hybrid composites via theoretical modeling and machine learning

Sanjida Ferdousi^{1,2}, Rigoberto Advincula^{3,4}, Alexei P. Sokolov⁵, Wonbong Choi^{2,6}, Yijie Jiang^{1,2*}

¹ School of Aerospace and Mechanical Engineering, University of Oklahoma, Norman, OK 73019

² Department of Mechanical Engineering, University of North Texas, Denton, TX 76207

³ Center for Nanophase Materials and Sciences, Oak Ridge National Laboratory, Oak Ridge, TN 37830, USA

⁴ Department of Chemical and Biomolecular Engineering, University of Tennessee, Knoxville, TN 37996, USA

⁵ Chemical Sciences Division, Oak Ridge National Laboratory, Oak Ridge, TN 37830, USA

⁶ Department of Materials Science and Engineering, University of North Texas, Denton, TX 76207, USA

* Corresponding author: Yijie.Jiang@ou.edu

Abstract

Hybrid composites combine two or more different fillers to achieve multifunctional or advanced material properties, such as lightweight and enhanced mechanical properties. The properties of the composites significantly depend on their microstructures, which can be tailored via advanced 3D printing processes. Understanding the process-structure-property relationships is critical to enable the design and engineering of novel hybrid composites for applications in aerospace, automotive, and protective coatings. Here, we develop 3D printable and lightweight hybrid composites and leverage the conventional design of experiments, a theoretical hybrid model, and an image-driven machine learning (ML) method to investigate their mechanical behaviors. The hybrid composites

are formulated with elastomer matrix, microfillers, and thin-shell particles, enabling a significant degree of design freedom of microstructures with densities and mechanical properties varying up to 70% and 91%, respectively. Our statistical analysis indicates that the 3D printing path direction and the microfibers fraction are dominating process parameters with contribution percentages of 45.3% and 57.7% on the specific stiffness and strength, respectively. A hybrid mechanics model is developed based on a simple Weibull distribution function and classical single-filler models to effectively capture the variations in mechanical properties, however, it overestimates the values due to its statistical constraints and idealization of experimental uncertainty. The image-driven ML model leverages the microscale images directly without losing the structural details, shows more accurate predictions with experimental data, and has 48.6% lower root mean square error than the theoretical model.

Keywords: hybrid composites, lightweight materials, convolutional neural network, 3D printing, hybrid mechanics model

1. Introduction:

A hybrid composite consists of two or more types of fillers, such as different geometries or functionality, incorporated into a matrix to attain enhanced multifunctional properties.^{1,2} Hybrid composites can have high specific properties and enhanced material performance in applications of aerospace, automotive, and other fields.³⁻⁵ Designed with diverse materials, hybrid composites can demonstrate particular characteristics, such as reduced weight, improved anti-fatigue properties, and high tensile strength and stiffness, due to their complex and heterogeneous microstructures.^{2,6} Lightweight hybrid composites can benefit flexible structural designs and multifunctional applications with low density and less energy consumption.⁷

With the advancement of 3D printing, the microstructures of composites can be carefully tailored by the control of manufacturing processes.⁸⁻¹¹ The mechanical properties of the composites highly rely on the intrinsic material properties of the fillers and matrix, such as fillers' geometries, densities, and strength, as well as resulting microstructures due to manufacturing processes, including spatial distribution, orientation, and alignment of the fillers.^{4,9,11-13} Leveraging the process-structure-property relationships, various works have been done with a focus on manipulating the spatial structural variation by 3D printing to achieve advanced composites with higher stiffness, toughness, and fatigue thresholds, which may have orders of magnitude enhancement.^{10,12-14} For example, Mo and Raney¹¹ harnessed a rotational nozzle and printing path designs to enable elongated and helical fiber alignments and created mechanical anisotropy by spatial distribution for aorta-inspired fiber composites. Mechanical properties contrast was obtained by printing a series of regions with various filler orientations.¹¹ In light of the design and manufacturing, the nature-inspired composites exhibited different deformation modes and high resistance to failure, even with significant defects and under cyclic loads. Another example is that Muth et al.¹⁰ 3D printed porous cellular structures and evaluated them with adjustable microstructures, geometries, and stiffness through the modification of ink composition, printing path, and sintering conditions. Compared to bulk-cast foam and light-based 3D printing structures, a unit cell based on these architected structures featured at least one order of magnitude less density and higher stiffness.¹⁰

To understand the processing of the advanced composites, it is important to establish the process-structure-property relationships and to correlate their mechanical properties with the heterogeneous and anisotropic structures and 3D printing processes. Conventional statistical methods, such as the design of experiments (DOE) and theoretical approaches, have been

investigated.^{12,15,16} In DOE, experimental planning, such as the Taguchi method, and analysis of variables (ANOVA) are used to quantify the process-property relations to optimize materials performance.^{17,18} Various techniques, such as morphological analysis, regression analysis, gray relational analysis, and tensile and rheological tests, are needed.^{15,19–21} This statistical approach requires prolonged experimental tests to acquire accurate results and is also limited to focusing on a significant feature. In theoretical modeling, various analytical models, such as continuum mechanics and micromechanical models, have been investigated for different material combinations and mechanical constraints.^{22–26} For instance, continuum mechanics models have been proposed to illustrate the phenomena, including the stretch-induced softening in elastomers-based composites and anisotropic damage parameters of the fiber reinforcement for the mechanical response of soft biological tissues, such as tendons and blood vessel walls.^{22,23,27,28} Micromechanical models, such as shear lag models and energy release rate calculations, were used to evaluate the shear stress distribution at filler-matrix interfaces and establish failure mechanisms.^{29,30} The field of structure-property relations has been explored based on statistical parameters derived from 3D printing processes or computational modelling, such as average filler dimensions, average orientation angles, roughness of interfaces, and average inter-filler distances.^{31,32} In order to investigate structure-property relationships, individual statistical parameters effect on mechanical behavior were generally discussed using constitutive and computational models.^{12,25,33} In addition, process parameters of 3D printing are also analyzed to identify and derive mechanical properties like stiffness, failure strength, damage behavior for the correlation of structure-property.³⁴ Despite the great effort in theoretical models, it remains challenging when different heterogeneous fillers are considered, or experimental uncertainties are considered rather than the ideal conditions.

Promising computational approaches based on advanced machine learning (ML) algorithms are emerging in composites studies, from nanoscale interface mechanics to large-scale structural designs.³⁵⁻³⁹ To evaluate the influence of composite mechanisms in additive manufacturing, a recent study developed a data-driven framework on composite systems using a regression ML model and compared that with conventional linkage techniques.³⁵ Similarly, other studies investigated the effects of structural design variables on flexural behavior using an ensemble learning data-driven model. They compared it with physics-based approaches and linear regression models, where the data-driven model achieved improved performance.³⁶ Further efforts were applied to establish the process-structure-property correlations considering their variables by developing a ML-based framework to demonstrate the ML model's efficiency and obtain controllable mechanical parameters.³⁷ Different than the data-driven models, fewer studies are using image-driven ML models, which could capture details of the microstructures direct from experimental observations and establish direct prediction based on the structure-property relationships. There are several types of image-driven ML models such as Convolutional Neural Network (CNN), Autoencoder, Recurrent Neural Network (RNN), Generative Adversarial Network (GAN), Support Vector Machines (SVM), Decision tree, Random Forest and so on.⁴⁰ However, most of the image-driven ML models are designed and adapted for generating, reconstructing, sequencing, and classifying images. In contrast, CNN is capable of recognizing images and extracting features from them. CNN provides scalable techniques for pattern recognition by utilizing the patches through whole images to identify the local features.^{41,42} The algorithm passes through several processing layers where it translates and relates image properties closer to the output at each step.⁴³ The current goal is to implement the CNN-based ML model to predict the mechanical properties from the experimental microstructure data, where it can

effectively correlate the structure-property relationships based on the local analysis of image features.

Here, we developed a composite mechanics model and an image-driven deep learning (DL) model to predict mechanical performances and understand the process-structure-property relationships. Different from conventional statistical approaches, we utilized experimental microstructure data in the ML model to forecast the factual mechanical characteristics of the composite by taking into account local defects, texture, and other deviations affecting the properties. In this work, we 3D-printed a series of lightweight hybrid composites. The heterogeneously structured composites were formulated with soft hyperelastic polydimethylsiloxane (PDMS) as matrix and hybrid fillers of glass microfibers and hollow thin shell microparticles. The composites were 3D printed using an extrusion-based direct ink writing (DIW) method. Combining the hybrid fillers was simple yet efficient, providing us composite design freedom with density and mechanical properties varying nearly two-fold quickly. To understand the relationships between process parameters and mechanical properties, we conducted the Taguchi method and statistical analysis on the ink compositions, 3D printing parameters, and the resulting experimental tensile testing data to identify the significant parameters for mechanical strength and stiffness. A theoretical mechanics model for the hybrid composites was developed based on a Weibull analysis that combined multiple classical single-filler composite models, incorporating the fraction and spatial information of the fillers and the failure criteria for the hybrid composites. Distinguishing from the conventional approach, we used an image-driven CNN deep learning method to capture the microstructural details directly from optical microscopy images and predict the critical mechanical properties. The image-driven model outperformed our statistical and theoretical analysis compared with experimental data.

2. Materials & Methods

2.1. Materials

Direct ink writing (DIW) 3D printing was used to print the hybrid PDMS-based composites. To formulate the 3D printable inks, mixtures of two types of PDMS, glass microfibers and hollow spherical particles, were used. For the matrix, PDMS from Dow Corning® SE 1700 (1:10 crosslinker ratio) and Dow Corning® Sylgard 184 (1:10 crosslinker ratio) were formulated at a ratio of SE1700:Sylgard184 = 10:1.5. The fillers were glass microfibers (FibreGlast® 38, initial length 123.1 ± 92.03 μm and diameter 11.7 ± 3.34 μm) and hollow spherical glass microparticles (FibreGlast® 22). We experimentally determined that the particles had a density of 0.13 ± 0.05 g/cm^3 based on casted composites with different particle fractions, an external diameter of 47.8 ± 1.33 μm by using optical microscopy, and a wall thickness of 160 ± 99.7 nm by calculations based on the external diameter and particle density. Volume fractions between 0-9% for each filler, respectively, were added to formulate different inks. The mixtures were mixed at 1600 rpm in a vacuum for 5 minutes in a bladeless planetary mixer (FlackTek, SpeedMixer™, DAC 400.2 VAC). The composite ink was then transferred into a 30cc syringe and centrifuged at 1400 rpm for 4 minutes to condense the inks and remove air bubbles.

2.2. Experiments

The loaded syringe was mounted on a home-built DIW 3D printer, which used a MakerGear® M2 platform and a high-precision Nordson® Ultra™ 2800 volumetric extrusion control system. Three different nozzle sizes (400, 610, and 800 μm) were used to extrude the materials. The extrusion rate was 0.0018-0.004 cc/s , and the printing speed was 10 mm/s . Tensile dogbone specimens with different thicknesses (0.6 to 1.2 mm) and printing directions (0°, 45°, and 90° against the

longitudinal direction of the tensile bars) were 3D printed. The printed composites were cured at 100 °C for 40 min. Microstructures were observed under an Amscope® MU1803 optical microscope at 10x magnification. At least 8 images of each printed specimen were taken for later use in ML studies. Uniaxial tensile tests were conducted in a universal testing machine (Shimadzu® AGS-X) at a constant nominal strain rate of 0.0067 1/s. Nominal stress-strain curves were then obtained from the force-displacement curves, and key mechanical properties, including stiffness, ultimate tensile strength, and toughness, were calculated for later analyses. The scanning electron microscope (FEI Quanta 200 ESEM) images of the cross section and top surface of the tensile tested specimen were shown in Fig. B.3 in SI Appendix B.

2.3. Taguchi method and ANOVA

Taguchi DOE method⁴⁴ was used to investigate the effect of process parameters on mechanical properties. There were four parameters, namely the volume fraction of fibers, the volume fraction of particles, printing direction, and nozzle size, and three levels each (Table B.1). An L9 orthogonal array was determined by the Taguchi method (Table B.1-2) and 4 specimens and mechanical tests were performed for each case. Statistical ANOVA analyzed experimental data on mechanical properties, including stiffness, strength, and toughness, with processing parameters.^{17,44} Significant tests using the F-test with a 95% confidence interval and the percentage of contribution for each process parameter were quantified (Table B.3 and B.4 in SI Appendix B).

2.4. Machine learning models

An integrated set of building blocks was used in CNN to systematically design, acquire, and extract the knowledge of features' spatial sequence from low-level to high-level patterns by employing backpropagation. CNN has the capability of learning and extracting meaningful features from

complex, high-dimensional images. The CNN model architecture also can identify the microstructural features while predicting the desired output with higher accuracy without the feature engineering that requires in other classical ML models.⁴⁵⁻⁴⁷ An image-driven CNN deep learning model was used to investigate the structure-property relationships.^{42,48} Details are in SI Appendix C.

In our models, five convolutional layers were used with 256, 128, 64, 32, and 16 numbers of channels/filters and (3,3) kernel/filter size with the same padding. The max pooling layer had a (2,2) filter size. A rectified linear unit (ReLU) was used as an activation function for all convolutional and fully connected layers. The nonlinear transformation ReLU function of $f(x) = \max(0, x)$ was used. After the convolutional layer, the data set was flattened and used in a single fully connected layer with 256 neurons. The output size was 1 with an input shape of (128,128,3). For training, mean square error (MSE) was used as a loss function and “adam” optimizer,⁴⁸ which was the extension of stochastic gradient descent to update the learning rate of each network's weight. To avoid overfitting, an early stopping method is used with the patience of the early stopping in 3 epochs to terminate the training after 3 epochs when the model performance has not improved. Here, validation loss was used as a monitor with a mode minimum to minimize the loss. To train the model, 100 epochs were utilized with 16 batch sizes. The whole dataset was split into three sets- training to fit the parameters to the model, validation to tune hyperparameters & validate the fitted model, and testing the dataset to validate the final model for unbiased evaluation. The total datasets were split into 85:15% for training and remaining, and the remaining datasets were divided into 85:15% for validation and testing.

By grid searching, the model was tuned using hyperparameters of the CNN, where the convolutional layers were varied. In the convolutional layer, the variation of the number of filters

was 512 to 16; filter/kernel size was 5 to 3. The filter size of the max-pooling layer was also changed from (4,4) to (2,2). The epoch was also tuned from 50 to 100 with 8 to 16 batch sizes. The model performance was validated based on the MSE. For the same 9 cases used in the Taguchi method and theoretical model, 77 samples were prepared, and each case had 8-9 samples. Each sample has 8 microstructure images taken uniformly distributed within the test areas. As a result, a total of 616 microstructural data as an input, along with the mechanical properties as an output, were used in the CNN model.

3. Results & Discussion

The overview of this study is illustrated in Fig. 1. Our work includes three parts, specifically (i) conventional statistical analysis using Taguchi and ANOVA, (ii) development of a hybrid theoretical mechanics model, and (iii) establishment of image-driven ML models. In the conventional statistical approach, we used the Taguchi method to optimize the number of experimental cases and ANOVA to quantify the contribution of several process parameters to the mechanical properties (Fig. 1a). Following that, a theoretical model for our hybrid composites was developed based on classical single-filler composites and Weibull distribution function (Fig. 1b). The mechanical behavior was explicitly correlated with the statistical structural parameters in this model. Finally, an image-driven CNN ML model was implemented to analyze the relationships between microstructures and mechanical properties to provide more accurate predictions for the 3D-printed hybrid composites (Fig. 1c).

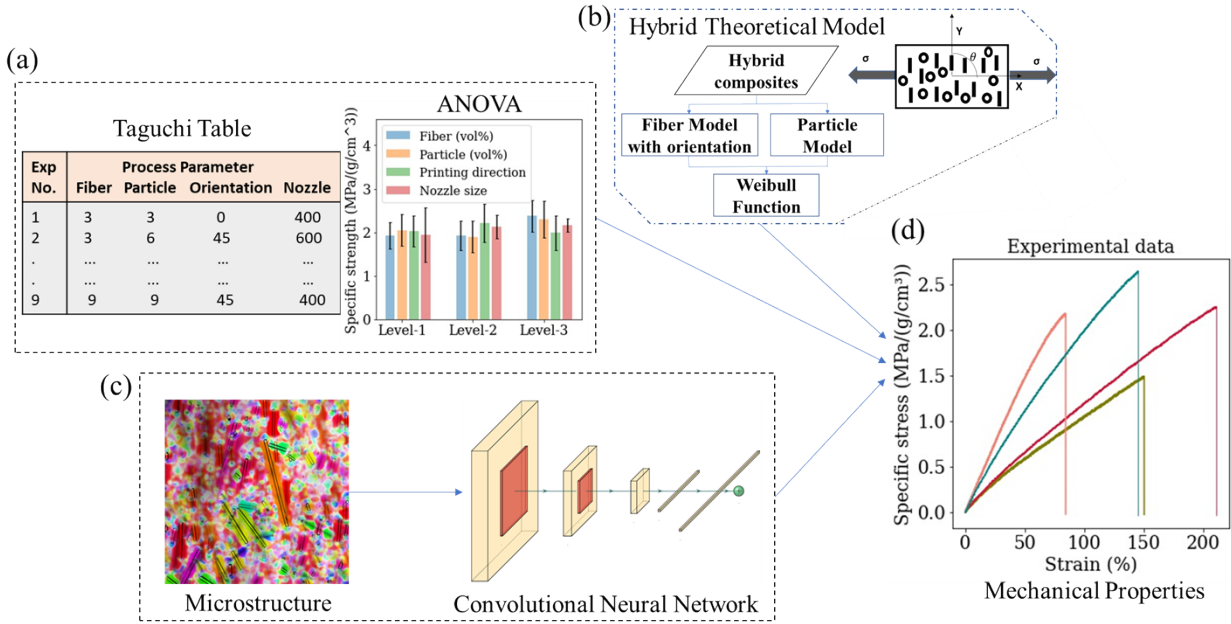


Fig. 1. An overview of the framework in this study for the 3D printed hybrid composites investigation. This framework includes (a) conventional statistical approaches to the design of experiments to quantify the effect of manufacturing process variables on mechanical properties, (b) a hybrid mechanical model, and (c) an image-driven ML model to capture (d) the experimental mechanical behaviors.

To fabricate the hybrid composites, we used the DIW method, which was a material extrusion-based additive manufacturing technique, to 3D print specimens of various ink formulas and printing directions (Fig. 2a). The fillers used in this study are shown in Fig. 2b, where the dimensions of the glass microfibers before mixing are $123.1 \pm 92.03 \mu\text{m}$ in length and $11.7 \pm 3.34 \mu\text{m}$ in diameter and the particle sizes are $47.8 \pm 1.33 \mu\text{m}$ in diameter with a shell thickness of $160 \pm 99.7 \text{ nm}$. The DIW method harnessed the rheological properties of the composite inks, specifically shear thinning and yielding (Fig. B.1 in Appendix B), to ensure smooth extrusion and retain shapes after printing.^{9,49} More importantly, the shear effect between ink flow and the nozzle walls results in the alignment of the fillers along the printing direction.^{9,16,50} By simply controlling

the printing path direction (Fig. 2c), different orientations of microfibers in composites could be achieved, as shown in Fig. 2d and Fig. B.2 (SI Appendix B). The geometric anisotropy of the microfibers would lead to mechanical enhancement and anisotropic responses for the composites. At the same time, the hollow spherical glass particles could provide local strength enhancement and enable the design freedom for desired nominal density of the hybrid composites. By tuning the volume fractions of the hybrid fillers, Fig. 2e shows the design space of the theoretical composite density (lines) and experimental validations of 3D printed samples (dots). Due to the low nominal density of 0.13 g/cm^3 of the thin-shell particles, the density of the hybrid composites could vary more than 70%, potentially enabling lightweight applications like energy absorption and protective coatings.

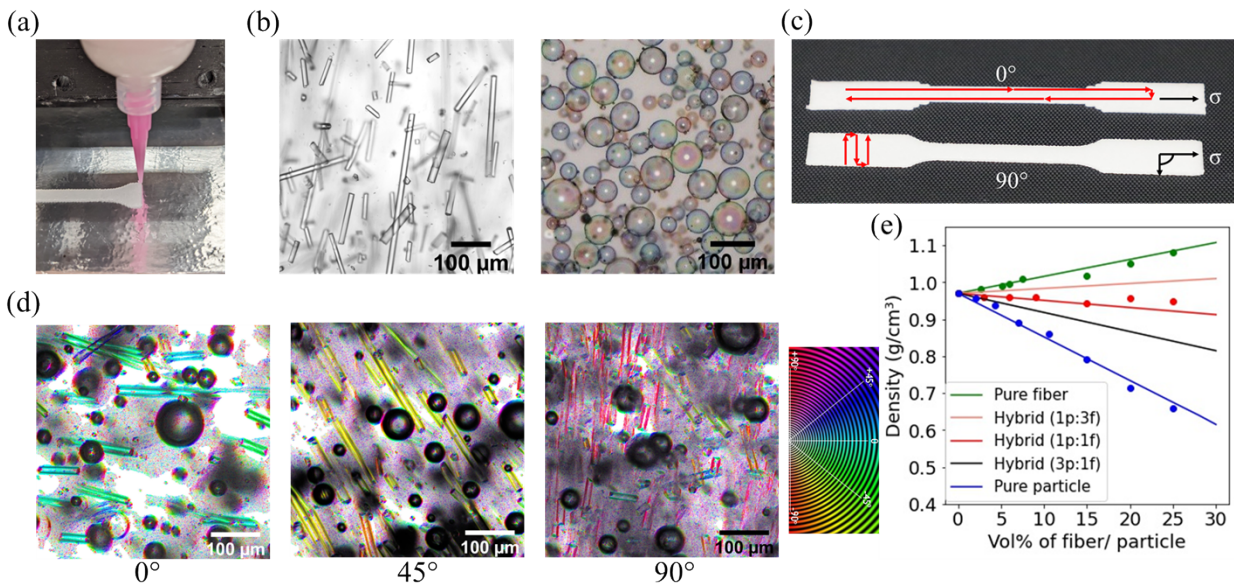


Fig. 2. (a) 3D printing of hybrid composites into a tensile specimen using the DIW method, (b) fillers in the printed composites, including glass microfibers and glass thin-shell spherical particles, (c) 3D printed tensile specimens with 0° and 90° printing directions, (d) microstructures of 3D printed hybrid composites with 0° , 45° and 90° printing directions along with their color definition, and (e) the nominal density range of the hybrid composites via the combination of fillers

at different volume fractions, where lines are the theoretical calculations and dots are 3D printed experimental validations.

To understand the correlations between the process parameters and mechanical properties, we first utilized the statistical Taguchi analysis and ANOVA. Tensile specimens were 3D printed in 9 cases with printing conditions listed in the Taguchi orthogonal array (Table B.1 in SI) and were used to collect mechanical properties from tensile tests. Fig. 3 illustrates the ANOVA results of the contribution percentages of four process parameters and specific stiffness and strength at different levels of these parameters. For stiffness, the printing direction had the highest percentage of contribution (45.3%) compared to the other three parameters (Fig. 3a). In addition, the stiffness for each level of process parameter was calculated using the Taguchi table (SI Table 1) in Fig. 3b. For printing direction, the stiffness was increasing 91.1% from level 3 to level 1, where the level 3 represents the printing direction of 90°, and level 1 represents 0°. The stiffness changes for the fiber volume fraction from level 1 to level 3 significantly increased by 64.3%, where level 1 represents 3 vol% of fiber and level 3 represents 9 vol%. For the volume fraction of particles, the stiffness improved by 55.9% from level 1 to level 3, representing the 3 and 9 vol% of particles. Fig. 3c illustrates the percentage of the contribution of each process parameter to the strength properties. And the tensile strength for each level of process parameters is visualized in Fig. 3d using the Taguchi table (SI Table 1). For the volume fraction of fibers, the average strength increased by 23.1% from level 1 (3 vol% fibers) to level 3 (9 vol% fibers). The average strength increased by 12.13% for the increasing volume fraction of particles from 3 to 9 vol%. The changes in strength and stiffness for nozzle sizes were determined as insignificant via an F-test (SI Table B.3 and B.4). The volume fraction of fibers dominated the percentage of contribution (57.64%) to the strength of the 3D printed hybrid composites.

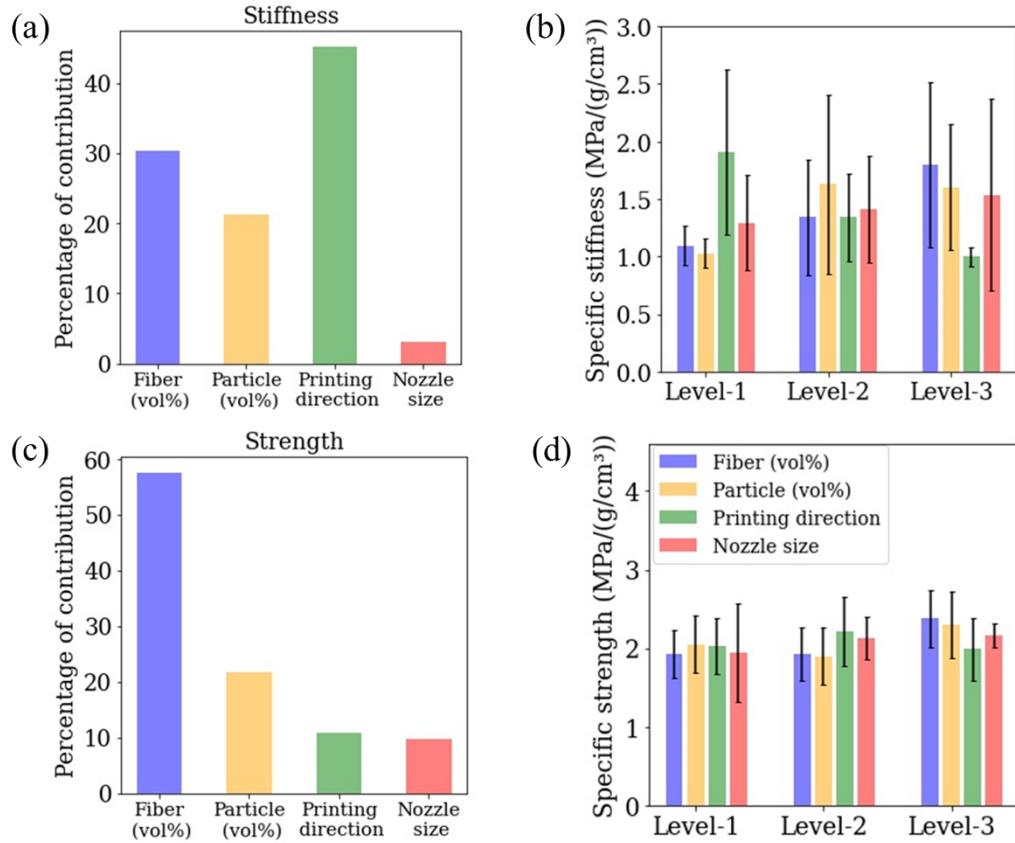


Fig. 3. The effect of process parameters on the mechanical properties of hybrid composites. (a) Percentages of contribution and (b) Taguchi analysis for process parameters on specific stiffness, (c) percentages of contribution, and (d) Taguchi analysis for specific strength at different levels of process parameters.

To further quantify the process-structure-property relationships, we developed a theoretical mechanical model to establish the properties based on the process parameters explicitly. Before getting the model for hybrid composites, we performed experimental validations on selecting multiple classical analytical models for single-filler composites (SI Appendix A). For the particle models, we used rigid inclusion, Mori-Tanaka, and Halpin-Tsai mechanics models based on Eq. (A.3), (A.4), and (A.5), respectively.^{26,51–54} For the fiber models, we applied the rule of mixture,

the Halpin-Tsai model, and the Tsai-Hill criterion to consider different fiber dimensions and orientations using Eq. (A.6).^{32,55–57} In Fig. 4a, we observed that the Mori-Tanaka particle model depicted an upper bound, and the Halpin-Tsai particle model was the lower bound.^{53,55} The rigid inclusion model aligned well with the experimental specific strength data, which increased linearly with particle volume fraction. For fiber-reinforced composites (Fig. 4b), the composites with transversely oriented fibers had less specific strength than the longitudinal ones. For all the cases, the specific strength depended mainly on the fiber sizes, which were highly correlated with the volume fraction of fiber¹² and the Halpin-Tsai and Tsai-Hill criteria fitted well with our experimental data.

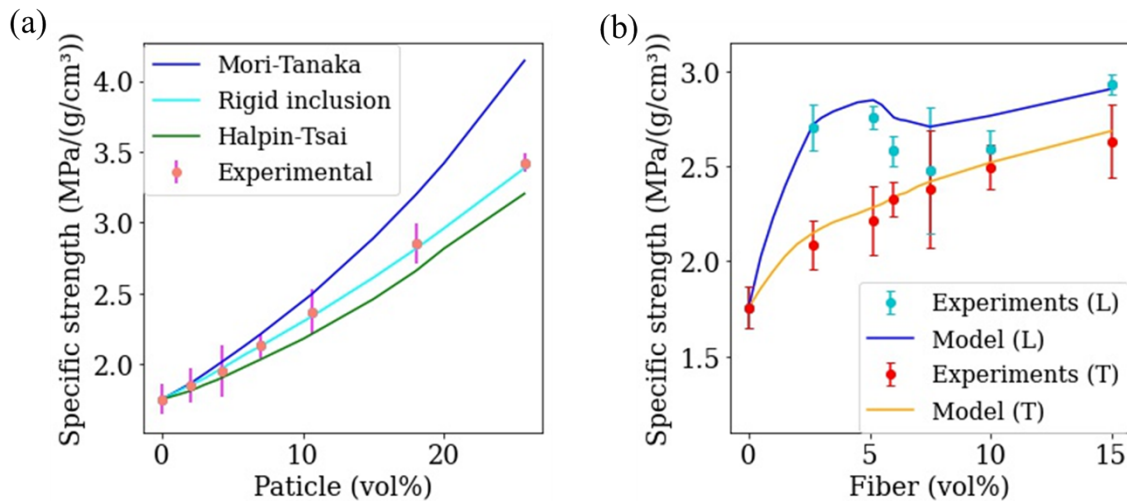


Fig. 4. Comparison of theoretical models with experimental data for single-filler composites. The specific strength of (a) glass particle reinforced composites for different volume fractions of particles using three different mechanics models and experimental data, and (b) glass fiber reinforced composites for different volume fractions of fibers with longitudinal (L) and transverse (T) fiber orientations using Halpin-Tsai fiber model and experimental data.

We developed a mechanics model for the 3D printed composites with hybrid fillers based on the single-filler composite models. A Weibull probability density function was used to incorporate the effect of microfibers and spherical particles on the specific strength.⁵⁸

$$\sigma_c = \sigma_{c_f} P_{c_f} + \sigma_{c_p} P_{c_p} \quad (1)$$

with

$$P_{c_f} = 1 + e^{\left(-\frac{l}{l_{cr}} \left(\frac{\sigma_{c_f}}{\sigma_{crf}} \right)^{m_1} \right)} \quad (2)$$

and

$$P_{c_p} = 1 + e^{\left(-\left(\frac{\sigma_{c_p}}{\sigma_{crp}} \right)^{m_2} \right)} \quad (3)$$

where σ_{c_f} is the strength of fiber composite, σ_{c_p} is the strength of particle composite, and l is the length of the fiber. σ_{crf} and σ_{crp} are the critical strength of fiber-matrix and particle-matrix interfaces, and l_{cr} is the critical length of fiber associated with the critical strength σ_{crf} . The key parameters to calculate the stress for hybrid models in Eq. (1) are the critical strengths of the filler-matrix interface, the critical length of fibers, and the variable m_1 and m_2 calculated using the weight function.⁵⁹ The strength of fiber and particle were calculated using the Mori-Tanaka and the Halpin-Tsai models combined with Tsai-Hill criterion formulas (Eq. (A.4) and (A.6)), respectively. The detailed derivation of the hybrid model is in the SI Appendix A.3.

Based on the hybrid model of Eq. (1), the specific strength of the composites was determined and compared with the experimental results shown in Fig. 5. Fig. 5a and 5b depict that the hybrid model captured the overall trend in the different cases, but with a propensity to overestimate the experimental results. The overestimation in the hybrid model is because the statistical method

disregards the structural details and has idealized assumptions without making allowances for experimental uncertainties, such as voids, geometric imperfection, and filament waviness during 3D printing.⁵⁰

To address the challenges above and provide better predictions, we harnessed a predictive image-driven CNN ML model to directly predict the critical mechanical properties using the microstructure of the hybrid composites. Using the CNN, we predicted the hybrid composites' stiffness, strength, and toughness from the composite's microstructures shown in Fig. C.1. The microstructural data contained detailed information, like volume fraction of fillers, shape, and sizes of fillers, geometric imperfections, inter-filament gaps, etc., to correlate with the mechanical properties, allowing the ML model to provide better predictions with higher accuracy.

Fig. 5a compares the experimental data, hybrid mechanical model results, and the CNN prediction results of specific strength. The ML prediction data showed close values against the experimental data. Error bars were associated with ML results since the specimens in each case (8-9 specimens in each case) had different local microstructures, which were fully considered in the ML model rather than being ignored or summarized in a statistical way as in the theoretical models. Rather than collecting an extensive dataset, our ML model required a minimal dataset of 616 images from 77 specimens for training. This saved much experimental effort and resulted in much higher accuracy. In Fig. 5b, an Ashby plot compares the theoretical model and ML model results of the mechanical strength of the hybrid composite to the experimental results. The error represents the waviness of the filament surface during 3D printing, which can be quantified through statistical measurement. The waviness is caused by variations in microstructure, processing conditions, and material composition. The error is defined in Eq. (4).⁵⁰

$$\sigma_e = \sigma_{exp}(1 + 6e^2) \quad (4)$$

Here, e is the experimental error, σ_{exp} and σ_e is the experimental strength and strength caused by the experimental waviness. In Fig. 5b, the red straight line indicates a perfect prediction with 0% experimental error, whereas 10% and 15% error represents the 10% and 15% experimental error due to the waviness. However, as expected, the waviness error is associated with statistical measurements and cannot explicitly define the local uncertainties. The theoretical model overestimated the strength, whereas the ML model data showed more accurate results with a Pearson's correlation coefficient 37.5% higher and a root mean square error (RMSE) 48.6% lower.

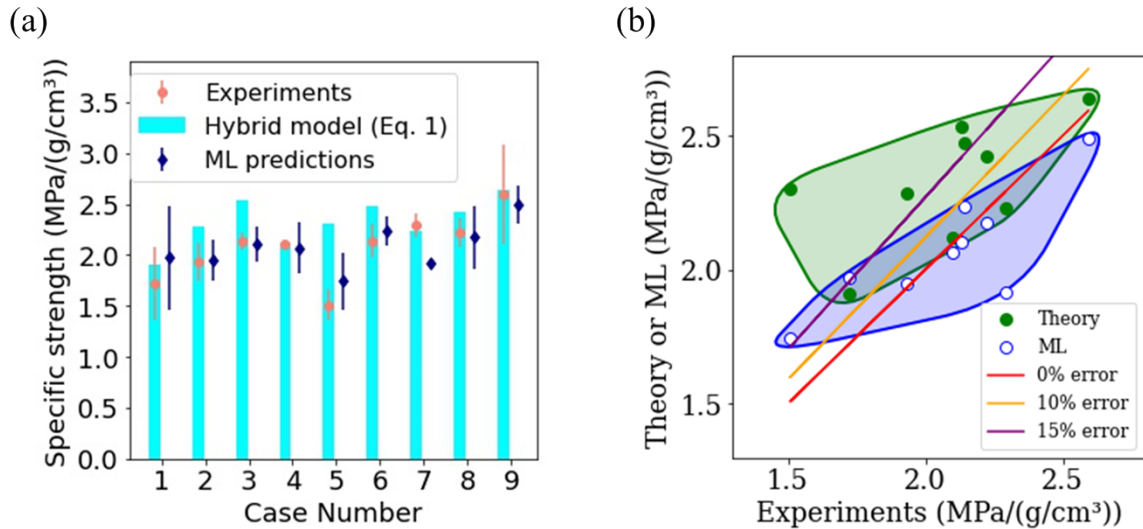


Fig. 5. (a) A comparison between the hybrid mechanics model, the experimental data, and the ML model prediction results of the specific strength of the hybrid composites, and (b) an Ashby plot of ML model predictions and the hybrid mechanics model of specific strength against experimental data.

Two demonstrations of impact and drop tests using the 3D printed hybrid composites and pure PDMS are shown in Fig. 6 and SI Movies S1 and S2. Both materials were 3D printed into a film shape with identical weights. Our drop tests used a dropping weight (5 lbs) from the same height (7.62 cm) onto a plastic ‘egg’ sandwiched by the hybrid composites and pure PDMS, respectively (Movie S1). The pure PDMS-protected eggs were broken into pieces (Fig. 6b). In contrast, the hybrid composite protected eggs had minimal damage on the top (Fig. 6a). In the impact test demonstrations, a high-speed rubber bullet hit the center of a thin rectangular plate of pure PDMS or hybrid composite at a constant speed of 1.43 m/s. The impact resulted in a deformation of the pure PDMS film of 6.9 mm, which was 62.7% larger than the hybrid composite film (4.24 mm), as shown in Fig. 6c-d and SI Movie S2. Both demonstrations showed the advantages of mechanical efficiency in energy absorption and deformation rigidity for our 3D-printed hybrid composites.

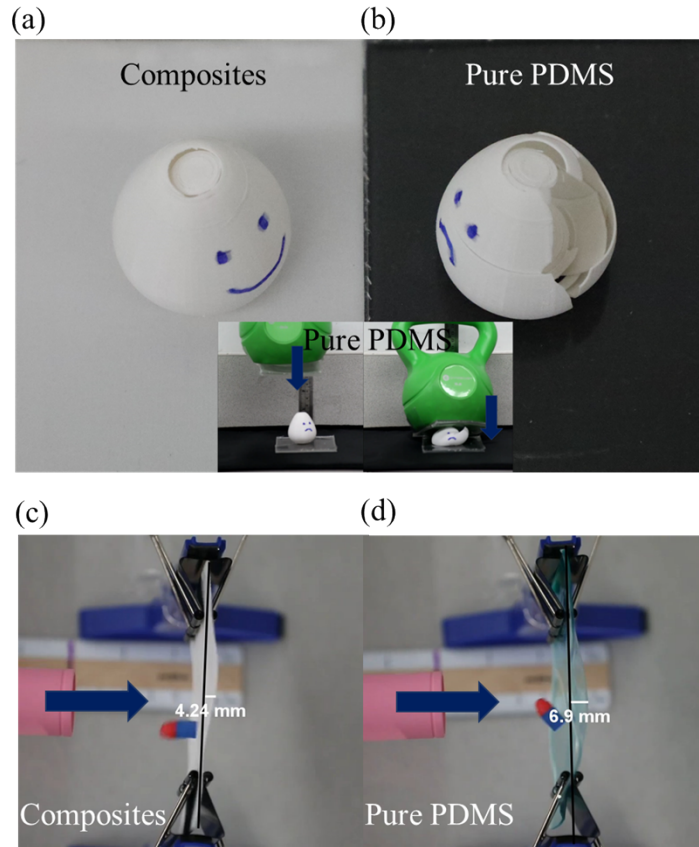


Fig. 6. Demonstrations of dropping tests using (a) the 3D printed lightweight hybrid composites and (b) pure PDMS films in protecting a plastic egg, and impact tests using (c) the hybrid composites and (d) pure PDMS films with identical weights.

4. Conclusions

We have developed 3D printable lightweight hybrid composites and investigated their process-structure-property relationships using conventional statistical approaches, theoretical modeling, and an image-driven CNN method. The hybrid fillers of solid microfillers and hollow particles provided greater degree of freedom in structural designs with reduced density and increased properties. Our statistical analysis determined the dominant parameters as the printing direction (contribution percentage of 45.3%) and the volume fraction of fibers (contribution percentage of 57.7%) on the specific stiffness and strength, respectively. A hybrid mechanics model was

developed in this study, harnessing a simple Weibull distribution function and classical single-filler models. This model could effectively capture the trend of the mechanical properties in different conditions but overestimated experimental results in general because the experimental local uncertainty was not considered in the model. The image-driven ML model predicted more accurate results with 48.6% lower RMSE than the hybrid theoretical model.

Credit author statement

Yijie Jiang performed the conception and design of this paper. Sanjida Ferdousi performed data processing, experimental data collection, and machine learning modeling. All authors contributed to the manuscript writing and revision. All authors read and approved the final manuscript.

Declaration of competing interest

The authors declare that they have no known competing financial interests or personal relationships that could have appeared to influence the work reported in this paper.

Acknowledgments

The authors acknowledge the support from the Vehicle Technologies Office (VTO) in the US Department of Energy (DOE), award number: Award VTO CPS 36928.

Data availability

Data will be made available on reasonable request. The online version contains supplementary information available.

Appendix: Supplementary data and two supplementary movies.

The following is the supplementary data to this article: [link...]

References

1. Jamir, M. R. M., Majid, M. S. A. & Khasri, A. Natural lightweight hybrid composites for aircraft structural applications. in *Sustainable composites for aerospace applications* 155–170 (Elsevier, 2018).
2. Gu, H. *et al.* Introducing advanced composites and hybrid materials. *Adv. Compos. Hybrid Mater.* **1**, 1–5 (2018).
3. Xie, C., Cao, M., Guan, J., Liu, Z. & Khan, M. Improvement of boundary effect model in multi-scale hybrid fibers reinforced cementitious composite and prediction of its structural failure behavior. *Compos. Part B Eng.* **224**, 109219 (2021).
4. Zhang, J., Chaisombat, K., He, S. & Wang, C. H. Hybrid composite laminates reinforced with glass/carbon woven fabrics for lightweight load bearing structures. *Mater. Des.* **36**, 75–80 (2012).
5. Bazan, P., Nosal, P., Wierzbicka-Miernik, A. & Kuciel, S. A novel hybrid composites based on biopolyamide 10.10 with basalt/aramid fibers: Mechanical and thermal investigation. *Compos. Part B Eng.* **223**, 109125 (2021).
6. Banerjee, S. & Sankar, B. V. Mechanical properties of hybrid composites using finite element method based micromechanics. *Compos. Part B Eng.* **58**, 318–327 (2014).
7. Cheng, P. *et al.* 3D printed continuous fiber reinforced composite lightweight structures: A review and outlook. *Compos. Part B Eng.* **250**, 110450 (2023).
8. Gu, G. X., Takaffoli, M. & Buehler, M. J. Hierarchically Enhanced Impact Resistance of

- Bioinspired Composites. *Adv. Mater.* **29**, 1700060 (2017).
9. Khatri, N. R. *et al.* Integrating helicoid channels for passive control of fiber alignment in direct-write 3D printing. *Addit. Manuf.* **48**, 102419 (2021).
 10. Muth, J. T., Dixon, P. G., Woish, L., Gibson, L. J. & Lewis, J. A. Architected cellular ceramics with tailored stiffness via direct foam writing. *Proc. Natl. Acad. Sci.* **114**, 1832–1837 (2017).
 11. Mo, C., Long, H. & Raney, J. R. Tough, aorta-inspired soft composites. *Proc. Natl. Acad. Sci.* **119**, e2123497119 (2022).
 12. Mo, C., Jiang, Y. & Raney, J. R. Microstructural evolution and failure in short fiber soft composites: Experiments and modeling. *J. Mech. Phys. Solids* **141**, 103973 (2020).
 13. Woo, R., Chen, G., Zhao, J. & Bae, J. Structure–Mechanical Property Relationships of 3D-Printed Porous Polydimethylsiloxane. *ACS Appl. Polym. Mater.* **3**, 3496–3503 (2021).
 14. Cipriani, C. E. *et al.* Structure-Processing-Property Relationships of 3D Printed Porous Polymeric Materials. *ACS Mater. Au* **1**, 69–80 (2021).
 15. Auffray, L., Gouge, P. A. & Hattali, L. Design of experiment analysis on tensile properties of PLA samples produced by fused filament fabrication. *Int. J. Adv. Manuf. Technol.* **118**, 4123–4137 (2022).
 16. Jiang, Y. & Raney, J. R. 3D Printing of Amylopectin-Based Natural Fiber Composites. *Adv. Mater. Technol.* **4**, 1900521 (2019).
 17. Mustapha, A. N. *et al.* Taguchi and ANOVA analysis for the optimization of the

- microencapsulation of a volatile phase change material. *J. Mater. Res. Technol.* **11**, 667–680 (2021).
18. Kowalczyk, M. Application of Taguchi and Anova Methods in Selection of Process Parameters for Surface Roughness in Precision Turning of Titanium. *Adv. Manuf. Sci. Technol.* **38**, 21–35 (2014).
 19. Yang, W. qiang *et al.* Designable Mechanical Properties of 3D Printing Composites with Multiple Filaments by Different Infill Percentages and Structures. *Adv. Eng. Mater.* **21**, 1900508 (2019).
 20. Das, A. *et al.* Rheological investigation of nylon-carbon fiber composites fabricated using material extrusion-based additive manufacturing. *Polym. Compos.* **42**, 6010–6024 (2021).
 21. El Magri, A., El Mabrouk, K., Vaudreuil, S. & Ebn Touhami, M. Experimental investigation and optimization of printing parameters of 3D printed polyphenylene sulfide through response surface methodology. *J. Appl. Polym. Sci.* **138**, 49625 (2020).
 22. Pena, E. Prediction of the softening and damage effects with permanent set in fibrous biological materials. *J. Mech. Phys. Solids* **59**, 1808–1822 (2011).
 23. Marini, G. *et al.* A continuum description of the damage process in the arterial wall of abdominal aortic aneurysms. *Int. J. Numer. Method. Biomed. Eng.* **28**, 87–99 (2012).
 24. Fu, S. Y., Feng, X. Q., Lauke, B. & Mai, Y. W. Effects of particle size, particle/matrix interface adhesion and particle loading on mechanical properties of particulate-polymer composites. *Compos. Part B Eng.* **39**, 933–961 (2008).

25. Martinez-Garcia, J. C. *et al.* A generalized approach for evaluating the mechanical properties of polymer nanocomposites reinforced with spherical fillers. *Nanomaterials* **11**, 830 (2021).
26. Liang, J. Z., Li, R. K. Y. & Tjong, S. C. Morphology and tensile properties of glass bead filled low density polyethylene composites: MATERIAL PROPERTIES. *Polym. Test.* **16**, 529–548 (1998).
27. Qi, H. J. & Boyce, M. C. Constitutive model for stretch-induced softening of the stress-stretch behavior of elastomeric materials. *J. Mech. Phys. Solids* **52**, 2187–2205 (2004).
28. Li, W. Damage Models for Soft Tissues: A Survey. *J. Med. Biol. Eng.* **36**, 285–307 (2016).
29. Ochiai, S., Hojo, M. & Inoue, T. Shear-lag simulation of the progress of interfacial debonding in unidirectional composites. *Compos. Sci. Technol.* **59**, 77–88 (1999).
30. López Jiménez, F. & Pellegrino, S. Constitutive modeling of fiber composites with a soft hyperelastic matrix. *Int. J. Solids Struct.* **49**, 635–647 (2012).
31. Yang, Z., Niksiar, P. & Meng, Z. Identifying structure-property relationships of micro-architected porous scaffolds through 3D printing and finite element analysis. *Comput. Mater. Sci.* **202**, 110987 (2022).
32. Zhao, Y., Chen, Y. & Zhou, Y. Novel mechanical models of tensile strength and elastic property of FDM AM PLA materials: Experimental and theoretical analyses. *Mater. Des.* **181**, 108089 (2019).

33. Tang, H., Chen, H., Sun, Q., Chen, Z. & Yan, W. Experimental and computational analysis of structure-property relationship in carbon fiber reinforced polymer composites fabricated by selective laser sintering. *Compos. Part B Eng.* **204**, 108499 (2021).
34. Papon, E. A. & Haque, A. Review on process model, structure-property relationship of composites and future needs in fused filament fabrication. *J. Reinf. Plast. Compos.* **39**, 758–789 (2020).
35. Gupta, A., Cecen, A., Goyal, S., Singh, A. K. & Kalidindi, S. R. Structure-property linkages using a data science approach: Application to a non-metallic inclusion/steel composite system. *Acta Mater.* **91**, 239–254 (2015).
36. Zhang, Z. *et al.* Predicting Flexural Strength of Additively Manufactured Continuous Carbon Fiber-Reinforced Polymer Composites Using Machine Learning. *J. Comput. Inf. Sci. Eng.* **20**, 061015 (2020).
37. Jiang, J., Xiong, Y., Zhang, Z. & Rosen, D. W. Machine learning integrated design for additive manufacturing. *J. Intell. Manuf.* **33**, 1073–1086 (2022).
38. Shah, V., Zadourian, S., Yang, C., Zhang, Z. & Gu, G. X. Data-driven approach for the prediction of mechanical properties of carbon fiber reinforced composites. *Mater. Adv.* **3**, 7319–7327 (2022).
39. Ferdousi, S. *et al.* Characterize traction–separation relation and interfacial imperfections by data-driven machine learning models. *Sci. Rep.* **11**, 14330 (2021).
40. Chowdhury, A., Kautz, E., Yener, B. & Lewis, D. Image driven machine learning

- methods for microstructure recognition. *Comput. Mater. Sci.* **123**, 176–187 (2016).
41. Yang, C., Kim, Y., Ryu, S. & Gu, G. X. Prediction of composite microstructure stress-strain curves using convolutional neural networks. *Mater. Des.* **189**, 108509 (2020).
 42. Herriott, C. & Spear, A. D. Predicting microstructure-dependent mechanical properties in additively manufactured metals with machine- and deep-learning methods. *Comput. Mater. Sci.* **175**, 109599 (2020).
 43. Kim, D.-W., Lim, J. H. & Lee, S. Prediction and validation of the transverse mechanical behavior of unidirectional composites considering interfacial debonding through convolutional neural networks. *Compos. Part B Eng.* **225**, 109314 (2021).
 44. Madhukar, P., Selvaraj, N., Rao, C. S. P. & Veeresh Kumar, G. B. Tribological behavior of ultrasonic assisted double stir casted novel nano-composite material (AA7150-hBN) using Taguchi technique. *Compos. Part B Eng.* **175**, 107136 (2019).
 45. Krizhevsky, A., Sutskever, I. & Hinton, G. E. ImageNet classification with deep convolutional neural networks. *Commun. ACM* **60**, 84–90 (2017).
 46. Wang, C., Tan, X. P., Tor, S. B. & Lim, C. S. Machine learning in additive manufacturing: State-of-the-art and perspectives. *Addit. Manuf.* **36**, 101538 (2020).
 47. Bhaduri, A., Gupta, A. & Graham-Brady, L. Stress field prediction in fiber-reinforced composite materials using a deep learning approach. *Compos. Part B Eng.* **238**, 109879 (2022).
 48. Kingma, D. & Ba, J. Adam: A Method for Stochastic Optimization. *Int. Conf. Learn.*

Represent. (2014).

49. Islam, M. N. & Jiang, Y. 3D Printable Sustainable Composites with Thermally Tunable Properties Entirely from Corn-Based Products. *ACS Sustain. Chem. Eng.* **10**, 7818–7824 (2022).
50. Compton, B. G. & Lewis, J. A. 3D-printing of lightweight cellular composites. *Adv. Mater.* **26**, 5930–5935 (2014).
51. Liang, J. Z., Li, R. K. Y. & Tjong, S. C. Tensile properties and morphology of PP/EPDM/glass bead ternary composites. *Polym. Compos.* **20**, 413–422 (1999).
52. Affdl, JC Halpin and Kardos, J. The Halpin-Tsai Equations: A Review. *Polym. Eng. Sci.* **16**, 344–352 (1976).
53. Mori, T. & Tanaka, K. Average stress in matrix and average elastic energy of materials with misfitting inclusions. *Acta Metall.* **21**, 571–574 (1973).
54. Hashin, Z. & Rosen, W. B. The Elastic Moduli of Fibre-Reinforced Materials. *J. Appl. Mech.* **31**, 223–232 (1964).
55. Tsai, S. W. & Wu, E. M. A General Theory of Strength for Anisotropic Materials. *J. Compos. Mater.* **5**, 58–80 (1971).
56. Egorikhina, E., Bogovalov, S. V. & Tronin, I. V. Determination of mechanical characteristics of unidirectional fiber composites. *Phys. Procedia* **72**, 66–72 (2015).
57. Yao, T., Zhang, K., Deng, Z. & Ye, J. A novel generalized stress invariant-based strength model for inter-layer failure of FFF 3D printing PLA material. *Mater. Des.* **193**, 108799

(2020).

58. Nelson, W. Weibull Analysis of Reliability Data with Few or No Failures. *J. Qual. Technol.* **17**, 140–146 (1985).
59. Barbero, E., Fernández-Sáez, J. & Navarro, C. Statistical analysis of the mechanical properties of composite materials. *Compos. Part B Eng.* **31**, 375–381 (2000).